18
Investigation of Network Phenomena in Hippocampal Slices Using Multi-Electrode Recording Arrays

Laura Lee Colgin

18.1 Introduction

It is commonly thought that higher cognitive functions in the brain are performed by groups of neurons working together as a network. Presumably, information in brain networks is represented by spatiotemporal patterns of neural activity. A technology that is useful for recording time-varying neuronal signals across spatially distributed brain regions is multi-electrode recording from brain slices. The traditional method of electrophysiological recording from brain slices is single-electrode recordings. Although single-electrode recordings are highly useful for studying synaptic physiology, their utility in network analyses is limited. Yet recording from multiple electrodes introduces additional complexities that may or may not, depending on the experimental conditions, be justified by the amount of information that they provide. The majority of this chapter is dedicated to two specific examples of fields of study that benefited from the use of multi-electrode recording: hippocampal rhythms, and temporally sustained and spatially distributed evoked responses. The second part of the chapter briefly addresses difficulties associated with multi-electrode recording and suggests ways that they may be overcome.

18.2 Applications of Multi-Electrode Recording

18.2.1 EEG Rhythms in Brain Networks

Rhythmic oscillations can be measured as classical electroencephalographic (EEG) waves that reflect the synchronized activity of ensembles of cells and thus provide a measure of neural activity at the level of neural networks. Rhythms have long intrigued researchers because they seem to be important for understanding how the forebrain becomes coordinated during different types of behaviors. Several lines of evidence support the idea that rhythms play an important role in cognitive processing and that particular frequencies subserve different functions.

The hippocampus exhibits three main bandwidths of oscillations: theta (4 to 7 Hz), beta (13 to 30 Hz), and gamma (~40 Hz; Leung et al., 1982). Theta is the best understood and most widely studied of the three, and results across different levels of investigation link theta to memory processing in the hippocampus. In a study of inhibitory avoidance learning, the magnitude of theta rhythm during the posttraining period was positively correlated with degree of retention (Landfield et al., 1972). Subsequent work showed that elimination of theta by lesioning or inactivating the lower brain region (medial septum/diagonal band) that generates the rhythm caused profound memory deficits in rats (Winson et al., 1978; Mizumori et al., 1990; M'Harzi and Jarrard, 1992). Afferent stimulation delivered in a manner that mimics theta is ideally suited for inducing long-term potentiation, a form of synaptic plasticity that is widely regarded as the substrate of many forms of memory (Larson et al., 1986; Larson and Lynch, 1986; Stäubli and Lynch, 1987). Stimulation on the positive phase of theta rhythm generates LTP in hippocampal slices and intact preparations (Pavlides et al., 1988; Bramham and Srebro, 1989; Huerta and Lisman, 1993; Hyman et al., 2003). Recently, magnetoencephalographic (MEG) arrays have recorded hippocampal theta oscillations in humans performing a well-known memory task (Tesche and Karhu, 2000; Jensen and Tesche, 2002).

The gamma rhythm has been the focus of much experimental work, yet its function remains controversial. Walter Freeman first proposed that gamma rhythms play an important role in sensory processing by allowing coherence to develop between spatially discrete areas (Freeman, 1975). Similarly, Wolf Singer and colleagues suggested that gamma rhythms transiently synchronize cells with disparate receptive fields, enabling individual aspects of a stimulus to be assembled into a coherent whole (Gray and Singer, 1989). Gamma rhythms occur in the entorhinal cortex in vivo (Chrobak and Buzsaki, 1998) and in vitro (van der Linden et al., 1999; Shimono et al., 2000), and gamma rhythms in the hippocampal pyramidal cell fields can be entrained by the entorhinal cortex (Charpak et al., 1995).

Beta rhythms have received less experimental attention. Both metabotropic glutamate receptor activation (Boddeke et al., 1997) and carbachol infusion (Shimono et al., 2000) have been reported to induce beta-frequency rhythms in hippocampal slices. Roger Traub and colleagues have published several reports of beta rhythms in hippocampal slices following tetanic stimulation delivered at twice-threshold levels (see Traub et al., 1999 for an example). It is unclear how closely these in vitro forms of beta correspond to beta waves in live animals. One problem is that some of the same experimental manipulations that induce beta activity in slices (i.e., carbachol infusion, metabotropic glutamate receptor activation) produce gamma rhythms under slightly different experimental conditions (Whittington et al., 1995; Fisahn et al., 1998). Still, mechanisms of beta rhythm production in the intact hippocampus fit relatively well with the characteristics of the in vitro waves. According to the explanation proposed by Leung (1992), pyramidal cells are excited by a combination of afferent stimulation and tonic depolarizing input provided by lower brain regions such as the medial septum. The excited pyramidal cells

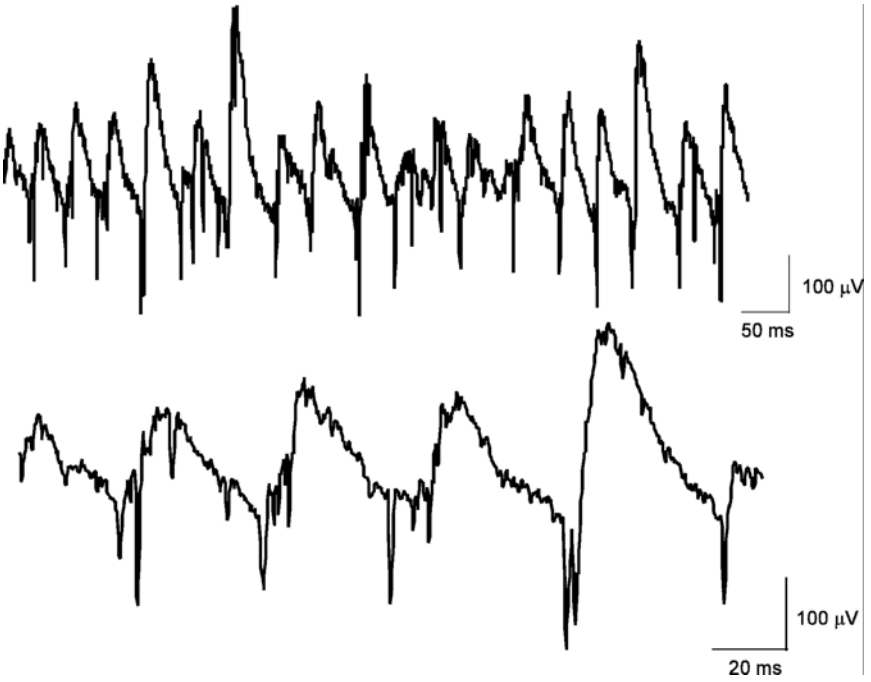

FIGURE 18.1. Carbachol-induced beta waves in hippocampal slices. Carbachol was infused at a concentration of 20 μM. Recordings were obtained from CA3 stratum pyramidale using conventional single-electrode recording methods (see Colgin et al., 2003 for a description of experimental methods).

then activate interneurons, which in turn feed back to inhibit the pyramidal cells after some delay. This model is consistent with the short excitatory phase/slow inhibitory phase cycle that is observed for beta rhythms in slices (Figure 18.1; see also Boddeke et al., 1997, Figure 2b and Traub et al., 1999, Figure 5B).

Regardless of how closely these rhythms correspond to their in vivo counterparts, beta oscillations remain an important dynamic of network function and the evidence described above supports the conclusion that the hippocampus retains its ability to produce these activity patterns in vitro. Beta rhythms are thought to be generated by local hippocampal circuitry (Leung, 1992), but they are also reported to facilitate long-range synchrony across cortical regions (Kopell et al., 2000). Little experimental work has been done to elucidate how beta rhythms are generated or how they synchronize disparate brain areas. The following section describes experiments that implemented multi-electrode recording to investigate the distribution, propagation, and mechanisms of production of beta rhythms in hippocampal slices.

Figure 18.2 depicts an example of cholinergically driven beta waves. A hippocampal slice placed upon an array of 64 electrodes is shown in Figure 18.2A. A

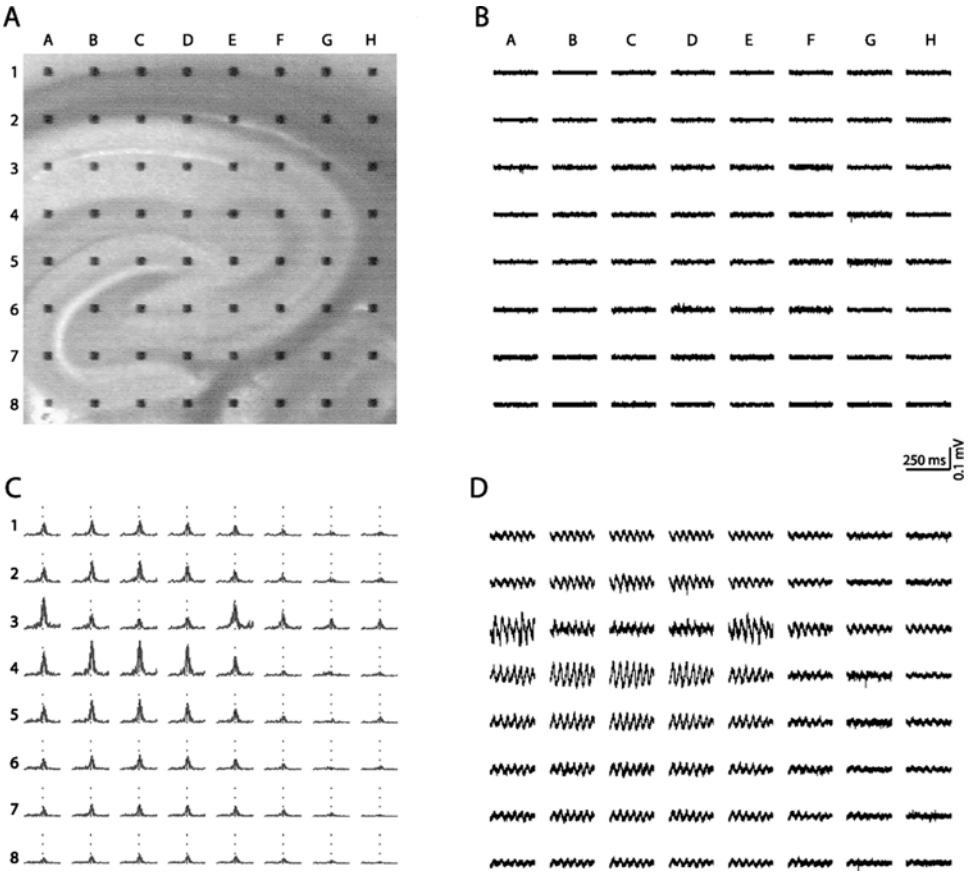

FIGURE 18.2. Carbachol-induced beta rhythms across 64 recording sites in a hippocampal slice. (A) Hippocampal slice placed upon an array of 64 electrodes (interelectrode spacing: 300 μm). (B) Spontaneous activity prior to carbachol infusion. Some minor single-unit activity was detectable, but no synchronized field activity was present. (C) Normalized power spectra computed for all 64 electrodes following infusion of 25 μM carbachol indicate that the dominant frequency was in the beta range and power was maximal in the apical dendritic field. Dotted line represents 26 Hz, the frequency at which power was maximal for this example. (D) Beta rhythms recorded after carbachol infusion. The waveform of the rhythms reversed across the cell body layer (e.g., electrode C2 vs. C4), indicating that they were locally generated. Amplitudes were large in the apical dendrites (e.g., electrode C4) and directly on the cell bodies (e.g., electrode E3). Calibration bars: 250 msec, 100 μV.

control recording of background activity from this slice reveals some spontaneous single-unit activity but no synchronized field potential oscillations or large amplitude activity of any kind (Figure 18.2B). Panel C shows the estimated power spectra across 64 electrodes for a two-second sample from the same slice following infusion of 25 μM carbachol. The dotted vertical line indicates the frequency at

which power was maximal for this particular case (26 Hz). Panel D illustrates the field potential oscillations for the time sample corresponding to the power spectra in panel C. As shown in both panels C and D, power was greatest in the apical dendritic fields and directly on the pyramidal cell bodies of field CA1. As expected, the phase of the rhythms was reversed across the cell body layer; this is evident in the traces from electrodes C2 and C4 in panel D.

The origins and distributions of cholinergic beta rhythms in vitro were investigated in an earlier study using two-dimensional current source density analysis of recordings from 64-electrode arrays (Shimono et al., 2000). Figure 18.3 was reproduced from that report and shows estimated currents in the hippocampus during one cycle of a beta wave. Initially, a weak current source (depicted in yellow) emerged in the stratum radiatum of field CA3 accompanied by diffuse, low-magnitude sinks (depicted in blue) near the stratum pyramidale. Over the next 6 milliseconds, a strong current sink developed in the apical dendritic field while intense current sources were simultaneously observed in the pyramidal cell layer and basal dendritic field. This pattern of activity then spread to field CA1 and was sustained for the next 12 milliseconds.

Six milliseconds later, at approximately 25 milliseconds from the start of the cycle, a current source surfaced in the apical dendritic region of CA3 with associated current sinks near the cell bodies and stratum oriens. This apical source–basal sink dipole then spread across the extent of CA1 and persisted for the next 15 milliseconds. By 42 milliseconds after the start of the cycle, much of the coordinated activity had begun to dissipate. The brief apical sink-delayed apical source pattern described above was commonly observed across a large group of slices. The degree to which beta rhythms were more prominent in CA1 versus CA3 varied from slice to slice, however, supporting the idea that the waves are generated by local circuits.

Results from single-cell studies of carbachol's actions (Behrends and ten Bruggencate, 1993; Benson et al., 1988) and anatomical localization of muscarinic-type acetylcholine receptors in the hippocampus (Levey et al., 1995; Hajos et al., 1998) provide clues as to what the current sinks and sources shown in Figure 18.3 might represent. Carbachol blocks potassium currents in hippocampal pyramidal cells (Madison et al., 1987; Benson et al., 1988) thereby making these cells more excitable (i.e., more likely to spike). Carbachol additionally suppresses evoked inhibitory postsynaptic currents (IPSCs), an effect that probably contributes to the increased excitability of the pyramidal cell population, but at the same time enhances spontaneously occuring IPSCs (Pitler and Alger, 1992; Behrends and ten Bruggencate, 1993). These results suggest that cholinergic stimulation differentially affects two populations of inhibitory interneurons, an idea that is consistent with anatomical studies showing that M2 muscarinic receptors are located on the dendrites and soma of interneurons that innervate the apical dendrites of pyramidal cells and on axon terminals near the pyramidal cell layer (Levey et al., 1995; Hajos et al., 1998).

Taken together, the above results support the following model of carbachol-induced beta rhythm generation (introduced in Shimono et al., 2000). Pyramidal

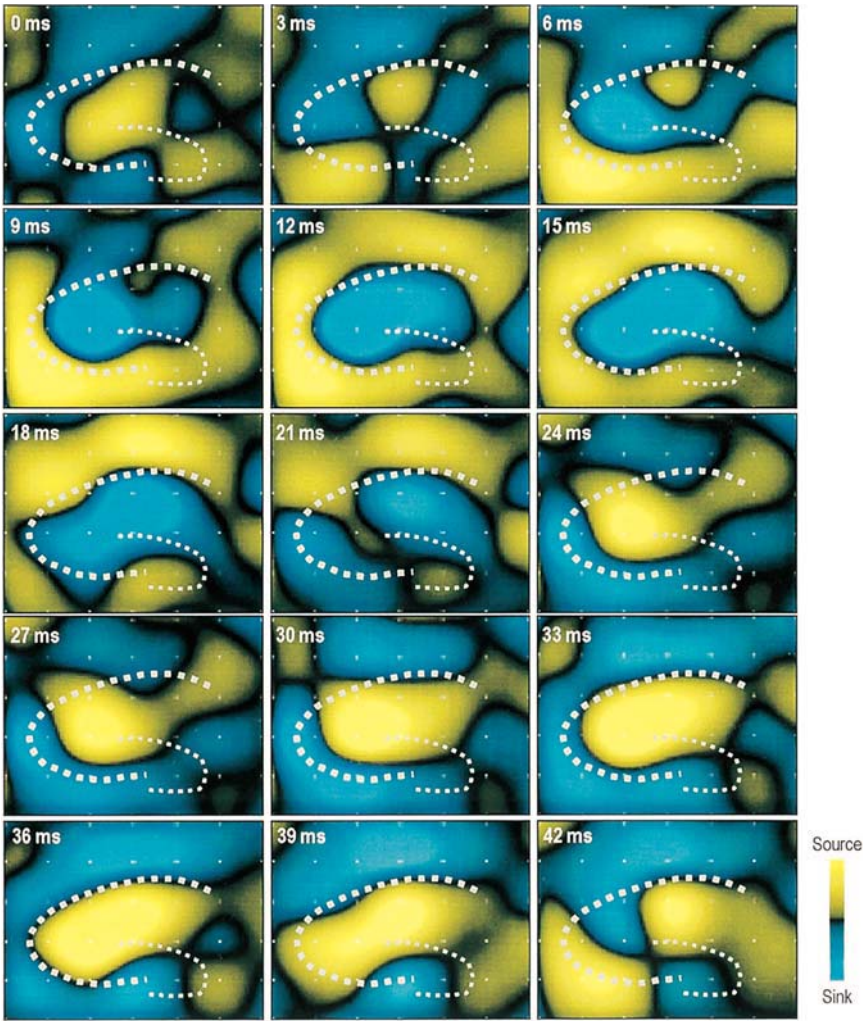

FIGURE 18.3. Evolution of current source density over time during one cycle of a beta wave. Each frame shows the instantaneous current source density computed at a particular time (indicated at the top left of each frame). Recordings were taken from 64 sites in the hippocampal network using a broad array of electrodes (interelectrode spacing: 450 μm). Blue indicates current sinks and yellow indicates sources. The positions of the pyramidal and granule cell body fields are represented by white, dashed lines. At $t = 6$ msec, an intense sink formed in the apical dendritic field of CA3, accompanied by a current source in the basal dendrites. The sink spread into the apical dendritic field of CA1 at $t = \sim 12$ msec. Activity dissipated, and then at $t = 27$ msec, an intense current source began to form in the apical dendritic field of CA3, accompanied by a current sink in the basal dendrites. The apical source coupled with its basal sink then spread to CA1 (~33 msec). The dipoles dissipated at 42 msec, and the cycle began anew. (Reproduced with permission from Shimono et al., 2000; © 2000 by the Society for Neuroscience.)

cells, tonically excited by blockade of potassium currents and suppression of inhibition at the soma, fire and spread their activity via the dense associational projections in field CA3 and collateral projections to CA1, resulting in the excitatory phase of the beta wave. Pyramidal cell firing activates a population of highly excitable interneurons that feed back to the apical dendrites of pyramidal cells, resulting in a strong inhibition in that region reflected as the inhibitory phase of the beta cycle. It is important to note that this model of beta rhythm production in slices fits well with mechanisms proposed for beta rhythm generation in freely moving animals (Leung, 1992).

The above description raises a critical experimental question regarding rhythms and their function in the hippocampal network: does the induction of rhythms shift the relative potencies of hippocampal afferents? As outlined above and described previously (Shimono et al., 2000), beta oscillations appear to be driven in part by inhibitory postsynaptic potentials (IPSPs) in the apical dendrites of pyramidal cells. This may result in a situation in which more distal afferents, such as the perforant path, are placed at a relative disadvantage to afferents terminating near the cell body and in the basal dendrites. This is likely not the operating mode when beta rhythms are absent. This suggests that the presence of rhythmic states serves to control the processing state of the hippocampal network. Empirical exploration of these topics using multi-electrode recording is described in the next section.

18.2.2 Beta Waves Can Affect the Size, Duration, Distribution, and Variability of Hippocampal Responses to Excitatory Inputs

The great majority of synapses in the hippocampus arise from associational and cortical afferents that use glutamate as a transmitter. As with other telencephalic areas, the hippocampus also receives significant projections from several subcortical structures that utilize an array of transmitters other than glutamate. The largest and best studied of subcortical projections to hippocampus is the cholinergic input from the medial septum/diagonal bands. Despite their relative sparseness, these afferents play an important role in the production of various rhythms in the hippocampus (Leung, 1992; Vertes and Kocsis, 1997; Leung, 1998). Less is known about how these inputs modulate hippocampal responses to activation of glutamatergic pathways and furthermore how responses are affected by ongoing rhythms. Cholinergic stimulation reduces the size of synaptic responses throughout most of the excitatory hippocampal pathways including the perforant path (Yamamoto and Kawai, 1967; Konopacki et al., 1987; Kahle and Cotman, 1989; Foster and Deadwyler, 1992; Colgin et al., 2003), CA3 associational system (Hasselmo et al., 1995), and Schaffer collaterals (Qian and Saggau, 1997; Hasselmo and Fehlau, 2001; Colgin et al., 2003), but the exact mechanisms responsible for the effects remain a source of controversy. Little to no work has been done to establish how cholinergic modulation of synaptic responses relates to cholinergically induced oscillations in hippocampus.

Several studies have shown that infusion of cholinergic agonists in hippocampal slices causes the near immediate appearance of rhythmic oscillations, but there is disagreement regarding the dominant frequency of the activity. Theta (4 to 7 Hz), beta (13 to 30 Hz), and gamma (~40 Hz) rhythms have each been reported to be triggered by application of carbachol (Konopacki et al., 1987; Huerta and Lisman, 1993; Williams and Kauer, 1997; Fisahn et al., 1998; Fellous and Sejnowski, 2000; Shimono et al., 2000; Colgin et al., 2003). In the Shimono et al. study using multielectrode recording (described above), carbachol elicited regionally discrete beta activity in the majority of slices. Results of two-dimensional current source density analyses pointed to the conclusion that bursts of pyramidal cell discharges, spread of excitation through collateral projections, and activation of apically directed feedback interneurons generated the beta waves (Shimono et al., 2000; see above for an in-depth description).

The above arguments make several predictions with regard to how cholinergic activation would affect hippocampal responses to stimulation of glutamatergic pathways. Minimally, responses occurring against a background of fluctuating excitation and inhibition should be notably different than those recorded under control conditions. This assumes that the oscillatory circuits proposed to be responsible for the beta activity actually engage a significant proportion of the hippocampal neuronal population. In addition, responses evoked in the presence of cholinergic oscillations should be much more variable than conventional field excitatory postsynaptic potentials (EPSPs) and in some regular fashion be affected by the phase of the beta wave. The experiments detailed in this section were intended to test these particular predictions and as well to provide specific information on how cholinergic activity alters the size, shape, and duration of excitatory responses. The results accord with the hypothesis that cholinergic inputs impose timing requirements on hippocampal afferents. Experimental methods and procedures used in the experiments described below were similar to those detailed previously by Shimono et al. (2000).

The widely hypothesized representation of information in brain networks is a spatially distributed, self-sustained pattern of activity. Yet in conventional hippocampal slice experiments, widely used for studying the physiology of the hippocampal network, evoked responses do not reverberate across time throughout the circuit. A traditional hippocampal evoked excitatory postsynaptic potential is a well-characterized, stereotyped response lasting on the order of tens of milliseconds (Figure 18.4). It consists of a fast, negative-going, depolarizing waveform resulting from glutamatergic excitation, and an after-hyperpolarization due to GABAergic inhibition. It is difficult to imagine how networks could retain information using this response, when many task cues are encountered serially with delays of hundreds of milliseconds between stimuli. An explanation is needed to bridge the gap between the time course of synaptic responses and the longer time course necessary for network operations. Novel results, described below, support the idea that stimulation in the presence of beta rhythms can elicit responses that extend across a substantial portion of the hippocampal network and are sustained for hundreds of milliseconds.

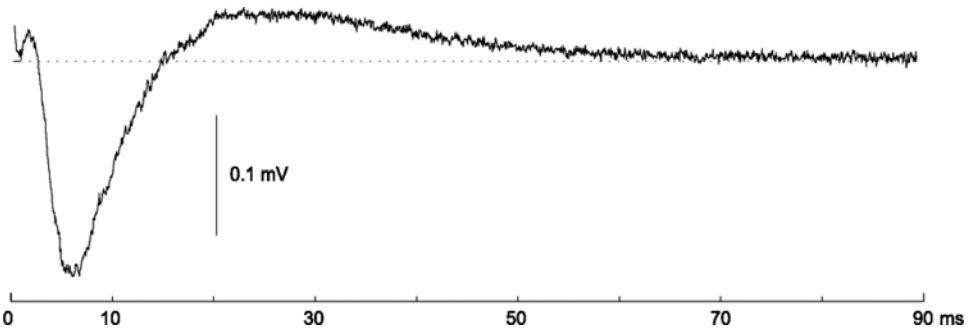

FIGURE 18.4. Example of a standard evoked potential in hippocampus. The initial negative-going waveform lasts approximately 10 msec, and is followed by a positive-going after-potential. This recording was taken from CA1 stratum radiatum in response to Schaffer collateral stimulation.

18.2.2.1 Laminar Profile and Regional Distribution of Sustained Network Response

Figure 18.5 compares an evoked response in the absence of rhythmic activity to a temporally sustained and spatially extended response evoked during cholinergically driven beta waves. As shown in Figure 18.5B, the dominant response in the control case was a rapidly developing and short-lived negative-going potential in the apical dendrites of field CA1 (e.g., electrode D2). This corresponds to the conventional field EPSP described in past physiological studies of the Schaffer-commissural (S-C) projections (see Figure 18.4). Responses elsewhere in the slice were much smaller than those recorded in field CA1. With the addition of carbachol, and subsequent generation of beta waves, two types of responses to single pulse stimulation emerged. In 16 of 53 recordings from eight slices, responses appeared similar to the control responses described above and are depicted in Figure 18.5C. However, in 37 of 53 traces from the same eight slices, carbachol produced two evident changes: single pulses triggered bursts of spikes in the stratum pyramidale of field CA3, and after-potentials became prominent features in both CA1 and CA3 (Figure 18.5D). An additional set of four slices was excluded from analyses because the delayed response was not observed in field CA1, most likely due to slight differences in slice preparation producing a weak CA3 $\rightarrow$ CA1 projection.

These effects can be seen more clearly in the single traces shown in Figures 18.6 and 18.7. The control response in field CA1, shown in gray, involved a typical biphasic response that reversed in polarity between the stratum radiatum (the terminus of the stimulated fibers; Figure 18.6, bottom) and the stratum oriens (Figure 18.6, top). The Schaffer-commissural response in field CA1 was greatly elaborated in the presence of carbachol (black traces, Figure 18.6). A sequence composed of a slow negative followed by a slow positive potential was added to the short latency field EPSP recorded in the apical dendrites (e.g., electrode E3 in Figure 18.5A).

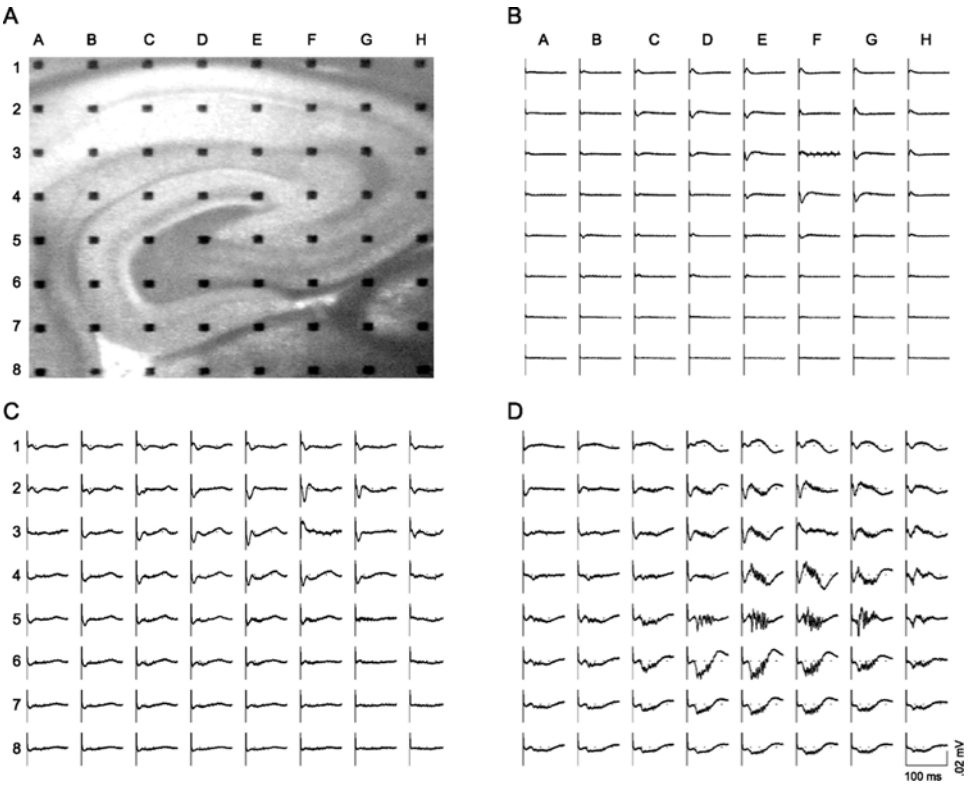

FIGURE 18.5. Evoked responses throughout the hippocampal network following stimulation of Schaffer collaterals in the presence and absence of carbachol-driven beta rhythms. Stimulation artifacts appear as a vertical line at the far left of each trace. (A) Hippocampal slice placed upon medium array of electrodes (interelectrode spacing: 300 μm). Electrode F3 was chosen for stimulation. (B) Evoked potentials across all 64 sites in the control condition. Note that responses did not propagate throughout the entire network. Activity was limited to the apical dendritic fields of CA3 (e.g., electrode F4) and CA1 (e.g., electrode E3). Phase reversals were prominent across the cell body layer in CA1 (e.g., electrodes E1 vs. E3). (C) Evoked potentials during carbachol-induced beta oscillations in an example in which a complex response was not generated. Responses and regional distribution were similar to the control condition. Background beta rhythm activity resumed almost immediately following stimulation. (D) Evoked response in the presence of cholinergic beta waves in an example in which a complex, reverberating response was generated. Initial fast negative-going potentials were observed in the apical dendritic fields of CA3 and CA1. However, instead of a prompt return to rhythmic activity, a sustained response was observed across the network. High-frequency cell spiking was recorded from CA3 pyramidal cells (e.g., electrode G5), presumably driven by an associated negative-going waveform in the basal dendritic field of CA3 (e.g., electrode E6). The apical dendritic field of CA3 exhibited a slow positive-going potential followed by a slow negative-going potential. The opposite apical-basal slow potential phase relationships were found in CA1. A delayed negative-going slow potential was recorded in the apical dendritic field of CA1 (e.g., electrode E3) with a corresponding delayed positive-going slow potential in the basal dendritic field (e.g., electrode E1). Note the increased spread of activation across the entire network during this complex response. Calibration bars: 100 msec, 200 μV.

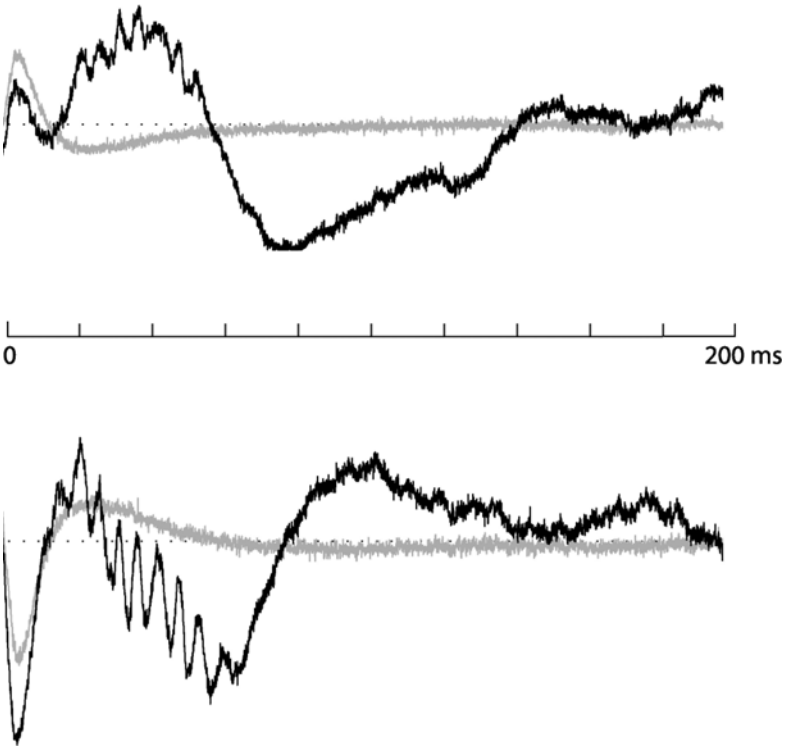

FIGURE 18.6. Evoked potentials in CA1 following stimulation of the Schaffer collateral pathway in the presence (black) and absence (gray) of carbachol-induced beta waves. The horizontal dotted line in the center of each trace denotes 0 μV. Stimulation in the absence of any rhythmic activity resulted in a stereotyped response (shown in gray), consisting of a fast negative-going potential followed by a positive-going after-potential in CA1 stratum radiatum (bottom) with a phase reversal of the response recorded in CA1 stratum oriens (top). The entire event was finished by 40 msec poststimulation. In the presence of cholinergically induced rhythms, a markedly different response was recorded (shown in black). In the apical dendritic field of CA1 (bottom), the primary fast response was followed by a sequence of slow potentials. The first was negative-going and was associated with high-frequency (∼100 to 150 Hz) spiking. The second slow potential was positive-going and did not return to baseline until 140 msec after stimulation. The response in CA1 stratum radiatum was phase-reversed in stratum oriens, such that a positive-going slow potential was followed by a negative-going slow potential and a return to baseline at ∼140 msec poststimulation.

The negative-going component, which began about 10 msec after the initial response and 25 msec after stimulation, was accompanied by evidence of high-frequency spiking. This was probably a reflection of activity in the pyramidal cell bodies in field CA3 because the spikes were largest in that region. Presumably, the delayed response in the apical dendrites of CA1 was due to prolonged spiking

of CA3 pyramidal cells reactivating the Schaffer collateral/commissural fibers (discussed in greater detail below). All components of the elaborated response in the apical dendritic terminal field of the Schaffer collateral/commissural fibers reversed polarity in the stratum oriens (black trace, Figure 18.6, top).

Carbachol-induced rhythms also had very large effects on evoked potentials recorded in field CA3 (Figure 18.7). The control response in the apical dendrites of CA3a was a typical field EPSP (Figure 18.7, bottom left, gray trace) and the corresponding basal dendritic area, stratum oriens, showed the expected polarity reversal (Figure 18.7, top left, gray trace). In the presence of the cholinergic beta rhythms, stimulation of Schaffer collateral fibers produced a complex polysynaptic response in CA3 that consisted of a positive-going slow potential in stratum radiatum that began while the monosynaptic EPSP was still present followed by a negative-going slow potential (Figure 18.7, bottom left, black trace). Note that the apical dendritic sequence of the slow potentials in CA3 (positive–negative) was opposite that observed in CA1. A phase-reversed version of the apical dendritic response occurred in the basal dendrites of CA3 (i.e., negative-going slow potential followed by positive-going slow potential; Figure 18.7, top left, black trace). Bursts of spikes accompanied the first of the carbachol-dependent slow potentials in CA3 (Figure 18.7, right panels, black traces); these were pronounced in the cell body layer and became reduced in amplitude with distance from that layer. The bursts had a frequency of at least ~100 Hz and began in the earliest phase of the first of the postmonosynaptic EPSP slow waves. Because bursts of cell firing must be accompanied by nearby depolarizing currents, the negative-going waveform in the CA3 basal dendrites associated with the cell spiking was most likely a depolarizing waveform (supported by current source density analysis; see below) driving the CA3 cells to fire repetitively. Prolonged firing of CA3 pyramidal cells presumably caused a secondary activation of Schaffer collateral fibers, resulting in the delayed, slow, negative-going potential recorded in CA1 stratum radiatum. Note that there was no cell spiking in the stratum pyramidale of CA3 under control conditions (Figure 18.7, right panels, gray traces).

Although detectable responses were virtually absent in fields CA3b and CA3c in the control condition, responses reverberated throughout the entirety of CA3 in the presence of cholinergic beta oscillations. Cell spiking was observed across the entirety of CA3 stratum pyramidale during an elaborated carbachol response (Figure 18.7, right panels, black traces). Not only were network responses more spatially distributed than control responses, they extended across a much longer time period. This topic is addressed in greater detail below.

The records shown in Figures 18.6 and 18.7 suggest that the slow responses driven by Schaffer collateral stimulation during cholinergic activation build up in field CA3 and then propagate into field CA1. Tests of this were carried out using the bursts of cell spikes described earlier. Highpass filtering the responses to remove slow synaptic potentials revealed that the bursts were larger in field CA3 than in field CA1 (Figure 18.8). Cross-correlations showed that the spikes in CA1 and CA3 were well correlated when the former were delayed by 2 to 4 msec from the latter, a value that accords well with the known conduction velocity of

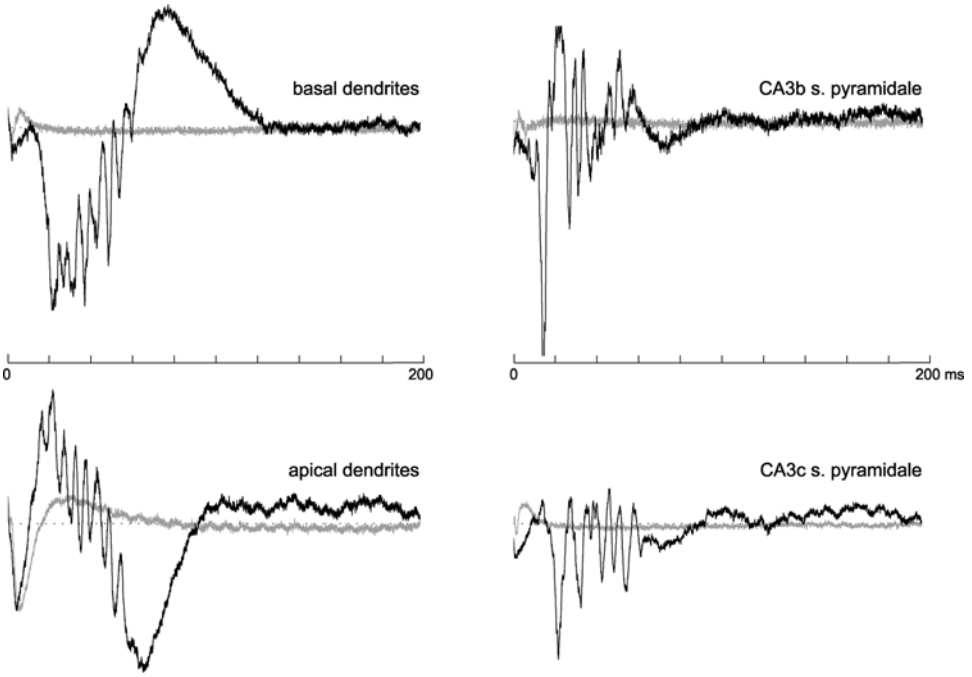

FIGURE 18.7. Evoked potentials in field CA3 in the presence (black) and absence (gray) of carbachol-driven beta rhythms following stimulation to the Schaffer collateral pathway. The dotted horizontal line in each trace indicates 0 μV. In the basal dendritic field of CA3 (top left), the control response (gray) was negligible, as was the fast component of the carbachol response. The initial phase of the slow potential of the carbachol response (shown in black) was a negative-going waveform with high-frequency spiking visible. The negative-going slow potential was followed by a positive-going potential, which returned to baseline at approximately 125 msec. In the apical dendrites (bottom left), a typical control response was recorded (shown in gray), consisting of a fast negative-going waveform followed by an after-hyperpolarizing potential. In the presence of carbachol (black trace), the apical dendritic response resembled the control response for a short time ($<$5 msec poststimulation) before veering off into a positive-going waveform ($\sim$10 msec poststimulation). Again, high-frequency spikes were visible during this phase. Note that the apical response was a phase-reversal of the basal response, such that the initial positive-going waveform was followed by a negative-going waveform. The source of the high-frequency spiking appeared to be the CA3 pyramidal cells (right traces, top and bottom), and spiking was observed across the entire extent of CA3 stratum pyramidale. Note that control responses (gray) in the cell body were insignificant. The negative-going waveform in the CA3 basal dendritic field was likely driving the high-frequency firing of CA3 pyramidal cells through the dense associational system of CA3.

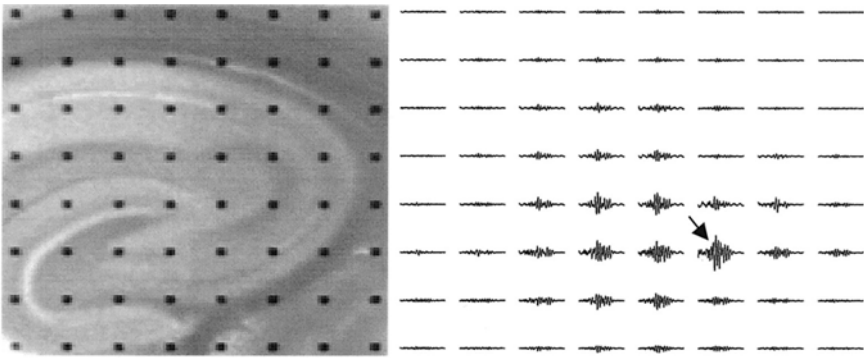

FIGURE 18.8. High-frequency bursting during complex response. A single stimulation pulse was delivered to the Schaffer collateral pathway following induction of beta rhythms by infusion of 25 μM carbachol. Responses recorded from the hippocampal slice depicted in the left panel were highpass filtered at 100 Hz to remove the slow potentials during the time segment from 10 to 80 msec after stimulation (right panel). It was evident that bursting was most prominent in field CA3, especially in stratum pyramidale (indicated by arrow). Calibration bars: 50 msec, 0.5 mV.

the Schaffer collateral projections from CA3 to CA1. These results confirm the idea that spiking bursts triggered by stimulation originate in field CA3 and then are propagated from there to CA1.

18.2.2.2 Time Course of Response

The minimum negative-going potential of the fast component occurred in the apical dendrites of field CA3 on average at 5.5 ± 0.7 msec after stimulation and in CA1 apical dendrites at 5.3 ± 1 msec (mean ± S.D., $n = 37$ stimulation trials from 8 slices). The minimum of the slow component of the CA3 basal dendritic negative-going potential occurred at 24 ± 10.5 msec after stimulation. In CA1, the minimum value of the slow, negative-going potential in the apical dendritic field occurred significantly later than its CA3 counterpart at 52.4 ± 19 msec poststimulation (paired *t*-test, two tails, $p < 0.0001$). The high degree of variance in the slow potentials was attributable to individual variations across slices. Also, the delayed potentials appeared to integrate multiple synaptic events, unlike the control monosynaptic EPSPs, thereby introducing additional degrees of variation.

The peak positive-going potential in CA3 apical dendrites corresponding to the slow negative-going potential in CA3 basal dendrites occurred at 17 ± 7.4 msec following stimulation. This peak was probably a source for the depolarizing currents in the basal dendrites but also likely reflected hyperpolarizing currents generated by feedback interneurons. Its maximum occurred at a significantly shorter time after the response than did the minimum negative-going slow potential in the basal dendritic field of CA3 (paired *t*-test, two tails, $p < 0.001$), indicating that the positive-going waveform was not merely a reversal of the basal dendritic

waveform. In addition, the time course of its peak was consistent with IPSPs generated by feedback interneurons in response to the primary fast response in the CA3 apical dendrites.

18.2.2.3 Response Size

The minimum amplitude of the fast negative-going potential was -60 ± 40 μV in the CA3 apical dendritic field and -70 ± 50 μV in the CA1 apical dendritic field. Neither of these values was significantly correlated with the minimum amplitude of the slow negative-going potential in CA1 apical dendrites (-105 ± 43 μV) nor the slow negative-going potential in CA3 basal dendrites (-180 ± 88 μV). On average, the minimum amplitudes of the slow components were more negative than the fast component minimum amplitudes (paired *t*-test, two tails, $p < 0.01$) for both CA3 and CA1. The average maximum amplitude of the large positive-going waveform in CA3 apical dendrites was 170 ± 135 μV. None of the amplitude measures were found to be significantly correlated with the power of the oscillations.

18.2.2.4 Current Source Density Analysis

Current source density analysis is a technique that is used to estimate the locations of the synaptic currents underlying field potentials (Nicholson, 1973; Haberly and Shepherd, 1973; Nicholson and Freeman, 1975; Nicholson and Llinas, 1975). The method was employed for the results described below in its continuous, two-dimensional form. This variant of current source density analysis has been previously described in significant detail (Shimono et al., 2000), so the description that follows is brief. The two-dimensional array of electrodes allowed for simultaneous estimation of current flows in any direction within the plane of the slice. Data were lowpass filtered at 100 Hz and spatially smoothed by a 3×3-weighted average kernel (0 1/8 0, 1/8 1/2 1/8, and 0 1/8 0). The result was then convolved with a 3×3 Laplacian kernel to obtain a discrete approximation of the second spatial derivative. Lastly, currents were obtained for all electrodes by calculating the 8×8 current source density for each time step and then estimating the value at each electrode location using bilinear interpolation.

One limitation of this technique is that only large spatial patterns with radii $\geq$ one-half of the interelectrode distance can be accurately resolved. Another problem is that lowpass filtering removes high-frequency data, thereby limiting the amount of fine detail that can be observed. Nevertheless, the method is quite useful for investigating spatially distributed events that change relatively slowly across time, and it could be argued that beta rhythms fall into this category as they are thought to involve synchronized activity across a large number of neurons.

Figure 18.9 shows the results of two-dimensional current source density analysis for selected time points in a 30 msec time window following stimulation to the Schaffer collateral pathway. The estimated current sinks (blue) and sources (yellow) are shown in the top four panels for the sustained network response in the presence of beta rhythms induced by carbachol and in the bottom four panels for an evoked response in the absence of cholinergic activity. At 4 msec poststimulation,

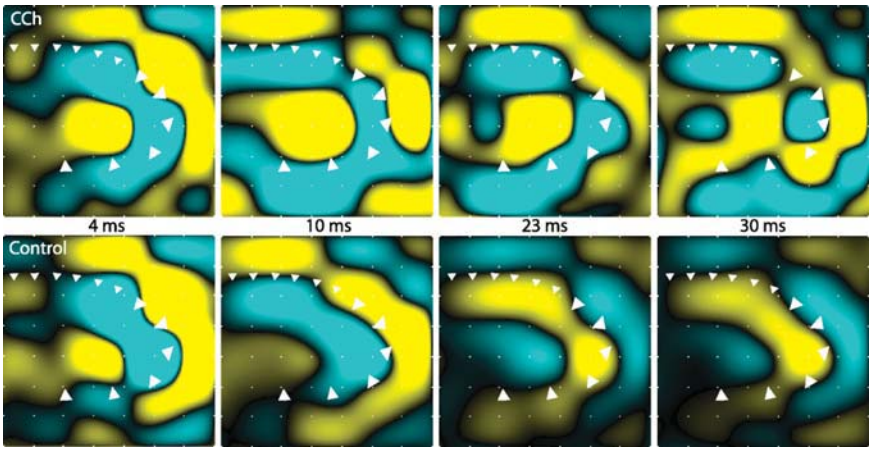

FIGURE 18.9. Two-dimensional current source density estimates for evoked responses in the presence (top) and absence (bottom) of carbachol-induced rhythms. Depolarizing current sinks are depicted in blue with hyperpolarizing current sources shown in yellow. The outline of the pyramidal cell bodies is depicted as white triangles, with larger triangles delineating field CA3 and smaller triangles for CA1. At 4 msec after a stimulation pulse was delivered to the Schaffer collateral pathway, differences between control and carbachol (CCh) responses were minimal. At 10 msec poststimulation during the CCh response, a large current source appeared in the apical dendrites of CA3 and a current sink appeared simultaneously in the basal dendrites, especially apparent in CA3c. In the control response, activity did not spread across the entirety of CA3 and the CA3 apical source/basal sink dipole was not present. At 23 msec, in the CCh case, the CA3 cell bodies and basal dendritic fields continued to be dominated by current sinks, and the CA3 apical source also remained. A prolonged depolarizing current sink was observed in the apical dendritic field of CA1 with a corresponding current source in CA1 stratum oriens. The control response, on the other hand, displayed weak activation at this time, with an after-hyperpolarization in the CA1 apical dendrites as the only distinguishing feature. This weak hyperpolarizing current source lingered in the CA1 apical dendrites of the control response at 30 msec, and stood in contrast to the strong depolarizing current sink observed in the same location at the same time point during the CCh response.

the responses were quite similar, although stimulation in the presence of cholinergic rhythms evoked a response that extended across slightly more of the network. In both cases, the major depolarizing current sinks occurred in the apical dendritic fields of CA1 and CA3. Corresponding current source dipoles were recorded across the cell body layers, but were not as prominent in the CA3 basal dendritic field for the carbachol response. Instead, it appeared that depolarizing currents were arising in the cell bodies of CA3 and beginning to produce a current sink. By 10 msec after stimulation, the entire network had fully mobilized in the carbachol case.

The two major differences between the response in the presence of carbachol-induced rhythms and the control response at this time were the appearance of a large current source in the CA3 apical dendrites and a well-formed current sink

in the CA3 basal dendrites during the carbachol response. In the control condition, the dipoles in CA3 were the same as in CA1 (apical sinks/basal sources), whereas the dipole relationships reversed in CA3 when cholinergic beta rhythms were present (CA3 apical source/basal sink, CA1 apical sink/basal source). It is also evident that the spread of activity was far greater when carbachol-induced rhythms were present than that seen without carbachol, particularly in field CA3 where the activity reached to the terminus of the pyramidal cell layer (i.e., field CA3c) in the carbachol case. Certainly related to greater spread, the intensity of activity was markedly increased in the presence of beta rhythms. At 23 msec following stimulation, the excitatory components of the evoked response were absent in the control condition, replaced by hyperpolarizing current sources in the apical dendritic fields of CA1 and CA3a. In contrast, the cholinergic response exhibited sustained excitatory current sinks in the apical dendrites of field CA1. Current sinks were also observed in the basal dendrites and cell bodies of CA3 at this time. At 30 msec poststimulation, the sustained apical current sink and its corresponding basal source in CA1 remained robust in the carbachol response, and only weak apical current sources lingered in the control condition.

Current source density analyses yielded consistent patterns in 7 of the 8 slices at time points approximately 5, 10, 20, and 30 msec following stimulation. At later time points, a large degree of temporal variability in the estimated currents developed across slices, probably due to timing variations in the slow potentials and the emergence of prominent high-frequency components likely reflecting cell spiking in CA3. Thus, simultaneous current source densities computed after 30 msec poststimulation are not discussed here.

18.2.2.5 Response Variability

There was an additional degree of variability that has not yet been discussed. Stimulation to the Schaffer collateral system in the presence of cholinergic rhythms elicited a sustained network response in approximately 70% of the stimulation trials, but in the other stimulation trials a response similar to a control EPSP was evoked. Field potential oscillations reflect alternating waves of excitatory and inhibitory currents. It follows that the oscillation phase, either excitatory or inhibitory, would predict whether a cell fires. As discussed above, depolarizing currents in the basal dendrites appear to be generating the sustained network response. Closer inspection of evoked responses in the presence of cholinergic beta waves indicated that the phase of the oscillations on which the stimulation pulse was delivered in the CA3 stratum oriens may have been responsible for the observed response variability. Analyses of seven slices revealed that in 34 out of 47 stimulation trials in which the network response was evoked, 18 stimulation pulses clearly landed on a local minimum in the basal dendritic field of CA3. In 11 stimulation trials in which the network response occurred, stimulation arrived when potentials in the CA3 basal dendrites were close to zero. Only 2 out of 13 recordings in which a sustained response was not generated in the presence of carbachol showed the

stimulation pulse arriving on a local minimum in the basal dendrites. In 5 recordings, it was difficult to determine where the stimulation pulse landed in the basal dendritic field because of degraded recording resolution likely due to volume conduction of activity. One slice was excluded from phase analysis because of this problem.

Figure 18.10 illustrates two responses to Schaffer collateral stimulation recorded from stratum radiatum of field CA1. The evoked response in the top panel was short lasting, and oscillatory activity resumed approximately 10 msec following stimulation. The stimulation pulse landed on a valley in the apical dendrites, which corresponded to a peak in the basal dendrites. In the bottom panel, the stimulation pulse landed on an apical peak in CA1, and a sustained network response was clearly evoked, disrupting rhythmic activity for over 200 msec. One measure of the magnitude of the prolongation of the response is the time it takes for the background beta oscillations to re-establish themselves. That is, physiological activity initiated within a group of neurons by stimulation of excitatory pathways should interfere with the production of rhythmic behavior by the same neurons. It is interesting to note that when stimulation arrives at a particular phase of ongoing rhythmic activity, one stimulation pulse to the Schaffer commissural projections is sufficient to block beta rhythms for at least 200 msec (Figure 18.10, bottom).

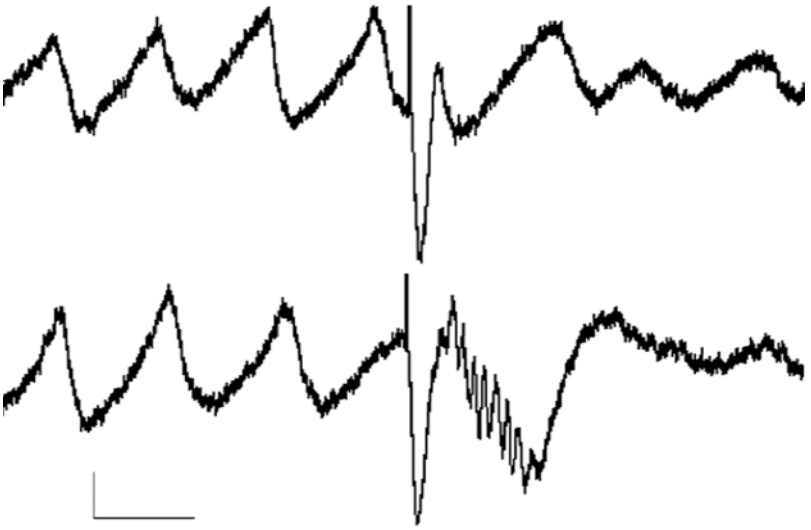

FIGURE 18.10. Within-slice variability of evoked responses in the presence of carbachol-induced oscillations. Recordings from CA1 stratum radiatum illustrate two examples of different responses to the same Schaffer collateral stimulation site (stimulation artifact seen as vertical line in center of trace). Note that in the top trace, stimulation arrived on an apical valley, and the response was not temporally sustained. In the bottom trace, stimulation was delivered on an apical peak, resulting in a temporally sustained response and subsequent disruption of rhythmic activity for ∼200 msec. Calibration bars: 50 msec, 200 μV.

18.2.2.6 Cholinergic Activation Can Increase Complexity of Responses to Glutamatergic Inputs

The above results suggest that cholinergic input to the hippocampus can profoundly affect responses generated by glutamatergic pathways in a way that has not been reported previously and in addition provide information as to the nature of the interaction. Responses to stimulation of the Schaffer collateral projections, the principal associational system of hippocampus, became much more complex than the standard field EPSP following the introduction of cholinergic rhythms. Although there was variability within slices, the predominant change was the addition of two slow potentials to the conventional field EPSP. In field CA1, the first of these was negative in the apical dendrites whereas the second was positive; both reversed across the cell body layer, indicating that they were locally generated. High frequency ($\sim$100 Hz) spike bursts accompanied the first wave. Given this and its location, it is reasonable to assume that the negative slow wave in CA1 reflected depolarization resulting from secondary activation of the Schaffer collateral projections. Additional evidence on this point is considered below. If the first slow wave was due to EPSPs sufficient to spike the CA1 pyramidal cells, then the delayed positive wave is likely to be an inhibitory postsynaptic potential (IPSP) set in motion by the excitatory inputs.

Slow waves corresponding to those just described were also recorded in field CA3 in the presence of carbachol-driven oscillations, but these did not have the same laminar profile observed in field CA1. That is, the first wave of the slow potential was positive in the apical dendrites and negative in the basal dendrites. The second wave remained opposite in polarity from the first, and the two potentials were reversed across the CA3 cell body layer. Somatic spikes riding on the first wave were of greater magnitude than those in CA1. From these observations it can be concluded that Schaffer collateral stimulation pulses in the presence of cholinergic activation can, at least on some trials, trigger secondary EPSPs that are sufficiently potent to cause high-frequency discharges of the CA3 pyramidal neurons.

By far the most probable source of the excitatory input is the massive CA3 associational system that, together with its commissural counterpart, generates the great majority of synapses in the subfield (Swanson et al., 1978; Ishizuka et al., 1990). The associational system densely innervates both apical and basal dendrites of the CA3 pyramidal neurons (Hjorth-Simonsen, 1973). It appeared that in the presence of beta rhythms, the basal dendritic system became dominant in CA3 during the slow component of the response. Anatomical and physiological evidence provide clues as to how this may have taken place. Muscarinic acetylcholine receptors are found on the dendrites and soma of a class of interneurons that projects to the stratum radiatum and also on axon terminals of basket cell interneurons at the stratum pyramidale/oriens border (Levey et al., 1995; Hajos et al., 1998). Physiological results support the conclusion that cholinergic stimulation facilitates the former group of interneurons while suppressing the latter (Pitler and Alger, 1992; Behrends and ten Bruggencate, 1993). Due to the carbachol-induced increase in

excitation of the apically projecting feedback interneurons, it is likely that the apical dendrites were hyperpolarized at the time the slow potential was initiated. This may have resulted in a situation where the basal dendritic associational system, released from basket cell inhibition by cholinergic stimulation, took control. This raises the possibility that subsequent inputs arriving in the basal dendritic field during this time may be treated preferentially over activation in the apical dendritic field. It is conceivable that sustained activation of this type, maintained primarily by reverberatory activity in the basal dendritic associational system of CA3, could serve to hold inputs for tens or hundreds of milliseconds.

As expected, the monosynaptic field EPSPs elicited by stimulation of Schaffer collateral fibers emerged at nearly the same time in CA3 and CA1 but cross-correlations showed that spike bursts associated with the temporally extended responses in CA1 were delayed by about 3 msec from those in CA3. This interval aligns with conduction and transmission delays for the Schaffer projections from CA3 to CA1. These observations combined with the location of the spike-associated slow wave in CA1 make it very likely that events in CA1 after the initial fast EPSP are driven by the delayed activation of the CA3 pyramidal neurons.

It will be noted that spike bursts emerged after, rather than in conjunction with, the monosynaptic CA3 response. Field EPSPs in CA3 were small and restricted in the "medio-lateral" axis, indicating that the fibers stimulated in CA1c did not form dense synaptic beds with a significant portion of the CA3 pyramidal cells. It appears then that a primary effect of cholinergic stimulation is to allow a relatively small starting population of neurons to set off spiking in cells throughout the CA3 region.

The dense associational system, to which each spiking cell would contribute, is well suited for generating reverberating activity but, as seen in the control cases, typically it does not. The spread of spikes and slow wave activity into those portions of CA3 adjacent to the dentate gyrus (CA3c) confirmed that the associational system had been activated by the Schaffer collateral/commissural projections in the presence of carbachol-induced beta waves. Physiological and anatomical studies together point to two muscarinic effects that are appropriate to produce such an outcome: a direct increase in the excitability of pyramidal neurons due to blockade of potassium currents (Nakajima et al., 1986; Madison et al., 1987; Benson et al., 1988), and suppression of release from feedback basket cells (see above).

It should be noted that the above arguments relate to the complex potential seen in the 10 to 100 msec interval following the monosynaptic field EPSP. The response often continued past this period as evidenced by a disruption of beta oscillations that on some trials lasted for 500 msec. Additional work is needed to identify the types of slow potentials associated with the extended response and to determine how they influence processing of glutamatergic inputs.

It is also important to point out that the effects described above have not been reported previously in a substantial body of literature concerning the effects of cholinergic agonists on responses elicited by Schaffer collateral stimulation. Instead, field excitatory postsynaptic responses to Schaffer collateral stimulation are widely reported to be suppressed by application of cholinergic agonists in

hippocampal slices, an effect that is thought to be presynaptically mediated (i.e., due to reduced glutamate release; Valentino and Dingledine, 1981; Sheridan and Sutor, 1990; Qian and Saggau, 1997; Colgin et al., 2003). In contrast, as discussed above, the effects reported here are likely to result from a combination of the postsynaptic effects of carbachol (i.e., tonic depolarization of pyramidal cells (Nakajima et al., 1986; Madison et al., 1987; Benson et al., 1988) and decreased GABA release from basket cell terminals (Behrends and ten Bruggencate, 1993). Potential explanations as to why these effects of cholinergic stimulation would not be detected in the majority of field-recording studies in slices but could be observed in the current work is discussed below.

18.2.2.7 Cholinergic Stimulation May Impose Timing Requirements on Glutamatergic Inputs

As described in earlier studies, and shown here, cholinergic stimulation elicits rhythmic oscillations in hippocampal slices. Various experimental approaches have established that the rhythms are produced by EPSP–IPSP sequences. The sequences are generated by the two effects noted above (i.e., increased excitability of pyramidal cells and decreased GABA release from basket cell terminals) acting together with a third cholinergic action, namely, increased excitability of a population of feedback interneurons that innervate the apical trees of the pyramidal neurons. Tonic excitation of the pyramidal cells (effect 1 above) occurring in the absence of basket cell inhibition (effect 2) results in increased spiking that quickly amplifies itself, via the CA3 collateral system, to the point that it triggers apically directed inhibitory feedback (effect 3). Spiking is shut down by the last event but then resumes as the feedback IPSPs dissipate.

This description does not describe in other than general terms the manner and degree to which the oscillatory activity might affect the primary hippocampal pathways. The novel results described above address this point and thereby raise the issue of whether, as has often been proposed, cholinergically driven rhythms impose timing requirements on the arrival of excitatory inputs. Post hoc analyses suggest that this may indeed be the case. That is, the magnitude and duration of the response to Schaffer collateral stimulation varied greatly across trials following the infusion of carbachol and subsequent production of beta rhythms with much of the variability attributable to the timing of stimulation pulses with respect to the beta rhythm phase. Thus, synchronization associated with beta waves may be a strategy for creating reliable and predictable time windows within which afferents arriving at opportune moments can exploit the processing capabilities of the network. These results suggest that some degree of synchronization would be needed between the hippocampus and its excitatory inputs.

The superficial layers of entorhinal cortex are the primary hippocampal afferent and are reported to generate beta waves when infused with cholinergic agonists (Shimono et al., 2000). Interestingly, the deep layers of entorhinal cortex, an important target of hippocampus and subiculum, produce gamma rhythms under the same conditions (van der Linden et al., 1999). Iijima and colleagues (1996)

reported that transfer of activity from the entorhinal cortex to the hippocampus was frequency-dependent, proposing that frequency-dependent transfer may be involved in selectively gating the entry of information into the hippocampus. Similarly, gamma activity has been reported to occur in hippocampus following carbachol infusion (Fisahn et al., 1998; Fellous and Sejnowski, 2000), and gamma coherence between hippocampus and entorhinal cortex is relatively high in vivo (Charpak et al., 1995; Chrobak and Buzsaki, 1998). In any event, hippocampus and retrohippocampal cortex appear to have sufficiently similar local circuits so that the cholinergic septal projections can provide the synchronization required by the beta activity.

18.2.2.8 Contributions of Beta Oscillations to Hippocampal Operations

Cortical rhythms are usually thought to synchronize afferents and thereby allow them to be more effective than would be the case if they arrived in a temporally scattered manner (e.g., Csicsvari et al., 1999). Other studies have shown that certain naturally occurring rhythms have deep relationships with synaptic plasticity (Larson et al., 1986; Staubli and Lynch, 1987; Pavlides et al., 1988; Huerta and Lisman, 1995; Lisman et al., 2001). The presently described results add to the list of potential functions of oscillations by showing that beta rhythms present windows of opportunity for afferents such that properly timed arrival of a modest input can result in a spatially and temporally extended response. With regard to the former, it is possible that the synchronization of large populations of cells that occurs during rhythms allows activity to spread more easily across a greater extent of a spatially distributed brain network.

As mentioned above, the results described here, obtained with a multi-electrode recording array, have not been reported in the numerous papers describing evoked responses in the presence of cholinergic stimulation. Cholinergic agents have only been reported to reduce monosynaptic evoked responses (Yamamoto and Kawai, 1967; Konopacki et al., 1987; Kahle and Cotman, 1989; Foster and Deadwyler, 1992; Qian and Saggau, 1997; Hasselmo and Fehlau, 2001; Colgin et al., 2003), but none of these studies involved stimulation in the presence of cholinergically driven rhythms. Thus, it may be the case that the cellular dynamics inherent in the rhythmic activity are in some way important to the production of temporally extended, polysynaptic responses of the type reported here. Alternatively, it is possible that some aspect of the multi-electrode array recording technique allowed these patterns to be seen. The worst-case scenario is that the slices used in the studies described above were not healthy and thus readily exhibited pathological responses for some reason potentially associated with the recording method.

However, it can be argued that an alternative explanation concerning the level of observation is more likely. Traditional slice-recording studies measure activity at the synaptic level whereas the phenomena described above are likely to reflect activity at a more macroscopic level involving ensembles of neurons acting

together as a network. There are several reasons to suspect that this may be the case. For one, the microelectrodes in the 64-electrode recording device (Panasonic; MED64) used in the experiments described here are 50 μm × 50 μm in size, substantially larger than the pulled glass micro-pipettes widely used in slice-recording studies. Also, the slice is placed on top of the electrodes in a small, fluid-filled dish. In this situation, the recording electrodes are separated from the source of the currents by several materials: the coating that the electrodes are treated with for slice adhesion, a thin layer of artificial cerebrospinal fluid (ACSF), and a layer of dead cells on the surface of the slice. This is in contrast to recordings from fine-tipped ("sharp") glass electrodes in which the recording electrode is lowered into the tissue as close as possible to the place where the currents are being generated thereby allowing for recordings that are detailed and spatially specific. In the case of multi-electrode arrays, the area between the electrodes and the source is filled with resistive media (i.e., layers of dead cells, electrode coatings). Under these conditions, currents diffuse out in this space, and thus only low frequency spatial features of the population activity will be recovered by the recording electrodes.

Because of these characteristics (large electrode size, distance between current source and recording site), a substantial degree of spatial averaging is part of the recording process. It may be possible that some low-frequency population events that are picked up by the large metal electrodes are obscured by random activity of individual cells in sharp electrode recordings. This explanation is more believable in the case of cholinergic stimulation in which individual cells have increased spontaneous firing rates. In any event, these arguments raise an important point: applications that are concerned with broadly occurring population events are more conducive to the use of multi-electrode recording arrays than are investigations at more microscopic levels.

It is important to be aware of these and other issues when conducting experiments with multi-electrode recording arrays. The previous section offered two examples of applications in which the small local activity that was lost in the diffuse and spatially smoothed signals recorded with multi-electrode recording arrays was compensated by the additional information gained by simultaneous recording of population events across spatially distributed sites. The next section addresses additional complications to be aware of when using multi-electrode recording arrays and suggests ways that these problems can be overcome.

18.3 Technical Considerations Associated with Multi-Electrode Recording

18.3.1 Low Spatial Resolution

The origins of signals recorded from multi-electrode arrays can be complicated to determine. After leaving their original source, currents diffuse out through many

layers of resistive media including dead cells, ACSF, and electrode coatings that essentially act as a lowpass filter. Much of the signal that remains will then be conducted with little to no degradation through the relatively large diameter, low impedance, metal recording electrode. Under these conditions, much of the locally occurring activity will be lost. On the other hand, broad synchronized population activity will be picked up, and in some cases will likely summate across time. Because of these factors, multi-electrode recording is best suited to applications involving investigation of large-scale ("network level") phenomena.

18.3.2 Volume Conduction

As noted above, there is a thin layer of conductive medium, namely, ACSF, between the source of the currents being measured and the recording electrode. Signals spread out through this medium away from their source and may be picked up by neighboring electrodes. This contributes to the aforementioned difficulty of localizing the sources of the recorded activity. It is thus necessary to examine recordings post hoc and verify that clear dipoles (i.e., phase reversals of the recorded signals) are observed and that negligible activity is recorded from electrodes that are placed under areas where one would expect to see little to no activity (e.g., hippocampal fissure). Volume conduction problems can be greatly minimized by taking all possible steps to ensure that the slice properly adheres to the electrodes (see Shimono et al., 2000 for details).

Current source density analysis can be used to alleviate both problems discussed above. It eliminates the effect of volume conduction and to a large extent reveals local synaptic activations. However, as was noted above, only spatially distributed currents with radii $\geq$ one-half of the interelectrode distance can be confidently estimated. Thus, in order to study more locally occurring currents, arrays with densely packed electrodes should be used (see Shimono et al., 2002, for an example).

18.3.3 Analysis Issues

Data collected with multi-electrode recording arrays can often be cumbersome. Visual inspection is required as a preprocessing step to ensure that signals have not been degraded as a result of volume conduction and/or improper adhesion of the slice to the electrodes. Even when signals are of high quality, each experiment generates a large amount of data: multiple signals (e.g., 64 in the examples above) for each time step. Inspection of complex spatiotemporal patterns present in the data is difficult because recording with the two-dimensional electrode grids generates three dimensions of information: the two spatial dimensions across time, a third dimension. Thus, it is often useful to collapse the various time series across disparate spatial locations into a single visual pattern, which may be viewed and analyzed more easily. Two-dimensional current source density analysis can accomplish this; with this method, all 64 signals are transformed into one coherent image for each

instantaneous time point sampled. However, it can still be difficult to compare these images across time and get a sense of the temporal order inherent in the signals.

Another option for simplification of multi-electrode data analysis is to employ 3-D visualization software, such as OpenDX, which enables transformation of the three dimensions of data into a single image. Although small details are lost with this method, meaningful patterns can emerge that are difficult to discern through other means. An example of 3-D visualization that was performed using OpenDX visualization software is shown in Figure 18.11.

In this example, each image represents 1500 msec-long, simultaneous recordings across 64 electrodes. The colors blue and yellow symbolize negative and positive voltages, respectively, with magnitudes of ± 0.012 mV. Image (1) shows a response to Schaffer collateral stimulation in the absence of cholinergic rhythms. Little to no spontaneous activity is present, and the response to stimulation is brief and spatially restricted. Image (2) is a visualization of a recording obtained in the presence of cholinergically induced beta rhythms. Rhythmic activity is apparent before and after delivery of the stimulation pulse, and the evoked response is spatially elaborate and temporally sustained. The bottom image (3) illustrates an example of a case in which a drug that positively modulates AMPA-type glutamate receptors (i.e., an "ampakine") was infused in combination with the cholinergic agonist carbachol, resulting in enhanced rhythmic activity. In this case, the response appears even more complex and prolonged and additionally is accompanied by high-frequency components. Comparison across the three experimental conditions in this example demonstrates the usefulness of 3-D

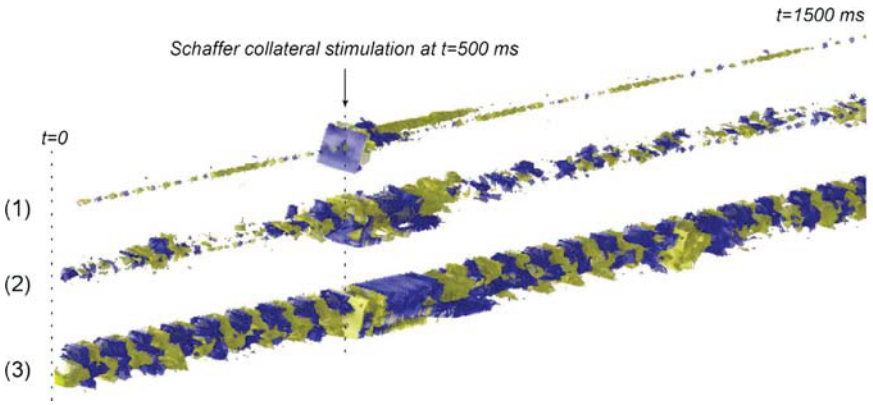

FIGURE 18.11. Overview of three complete time series (1500 msec in duration) visualized in three dimensions using OpenDX software. The three images represent: (1) control, (2) carbachol, and (3) carbachol + ampakine. Blue symbolizes -0.012 mV and yellow symbolizes $+0.012$ mV. The intermittent strand of positive voltage (yellow) seen in all three cases and especially apparent in (1) is an artifact due to the loss of recording capabilities at the site chosen for the stimulation electrode.

visualization methods. That is, through the use of 3-D visualization, one can tell in a glance that the three images are dramatically different.

18.4 Concluding Remarks

Tools that are capable of sampling electrophysiological signals across spatially distributed brain networks, such as multi-electrode recording arrays, will likely be used increasingly often as more and more researchers strive to bridge the gap between synaptic interactions and computations across neuronal ensembles. This chapter pointed out specific studies in which the increased dimensions of information provided by multi-electrode recording allowed spatiotemporal patterns to be observed that would have been difficult to discern using conventional recording methods. Although technical difficulties can complicate the use of multi-electrode recording, they can largely be overcome through sophisticated analysis techniques. As computational methods and the electronic devices themselves are advanced, further insights into the complex operations of brain networks are to be expected.

Acknowledgments. The writing of this chapter was funded by NIA Training Grant 5T32 AG00096-21. The author thanks Fernando A. Brucher for assistance with current source density analysis and helpful discussions, Gary Lynch for valuable comments on earlier versions of this work, Ken Shimono for help with multi-electrode recordings, and Cheryl A. Cotman and Linda C. Palmer for providing the 3-D visualizations depicted in Figure 18.11.

References

Behrends, J.C. and ten Bruggencate, G. (1993). Cholinergic modulation of synaptic inhibition in the guinea pig hippocampus in vitro: Excitation of GABAergic interneurons and inhibition of GABA-release. *J. Neurophysiol.* 69: 626–629.

Benson, D.M., Blitzer, R.D., and Landau, E.M. (1988). An analysis of the depolarization produced in guinea-pig hippocampus by cholinergic receptor stimulation. *J. Physiol.* 404: 479–496.

Boddeke, H., Best, R., and Boeijinga, P.H. (1997). Synchronous 20 Hz rhythmic activity in hippocampal networks induced by activation of metabotropic glutamate receptors in vitro. *Neuroscience* 76: 653–658.

Bramham, C.R. and Srebro, B. (1989). Synaptic plasticity in the hippocampus is modulated by behavioral state. *Brain Res.* 493: 74–86.

Charpak, S., Pare, D., and Llinas, R. (1995). The entorhinal cortex entrains fast CA1 hippocampal oscillations in the anaesthetized guinea-pig—Role of the monosynaptic component of the perforant path. *Euro. J. Neurosci.* 7: 1548–1557.

Chrobak, J.J. and Buzsaki, G. (1998). Gamma oscillations in the entorhinal cortex of the freely behaving rat. *J. Neurosci.* 18: 388–398.

Colgin, L.L., Kramar, E.A., Gall, C.M., and Lynch, G. (2003). Septal modulation of excitatory transmission in hippocampus. *J. Neurophysiol.* 90: 2358–2366.

Csicsvari, J., Hirase, H., Czurko, A., Mamiya, A., and Buzsaki, G. (1999). Oscillatory coupling of hippocampal pyramidal cells and interneurons in the behaving rat. *J. Neurosci.* 19: 274–287.

Fellous, J.M. and Sejnowski, T.J. (2000). Cholinergic induction of oscillations in the hippocampal slice in the slow (0.5–2 Hz), theta (5–12 Hz), and gamma (35–70 Hz) bands. *Hippocampus* 10: 187–197.

Fisahn, A., Pike, F.G., Buhl, E.H., and Paulsen, O. (1998). Cholinergic induction of network oscillations at 40 Hz in the hippocampus in vitro. *Nature* 394: 186–189.

Foster, T.C. and Deadwyler, S.A. (1992). Acetylcholine modulates averaged sensory evoked responses and perforant path evoked field potentials in the rat dentate gyrus. *Brain Res.* 587: 95–101.

Freeman, W. (1975). *Mass Action in the Nervous System*, Academic Press, New York.

Gray, C.M. and Singer, W. (1989). Stimulus-specific neuronal oscillations in orientation columns of cat visual cortex. *Proc. Natl. Acad. Sci. U. S. A.* 86: 1698–1702.

Haberly, L.B. and Shepherd, G.M. (1973). Current-density analysis of summed evoked potentials in opossum prepyriform cortex. *J. Neurophysiol.* 36: 789–802.

Hajos, N., Papp, E.C., Acsady, L., Levey, A.I., and Freund, T.F. (1998). Distinct interneuron types express m2 muscarinic receptor immunoreactivity on their dendrites or axon terminals in the hippocampus. *Neuroscience* 82: 355–376.

Hasselmo, M.E. and Fehlau, B.P. (2001). Differences in time course of ACh and GABA modulation of excitatory synaptic potentials in slices of rat hippocampus. *J. Neurophysiol.* 86:1792–1802.

Hasselmo, M.E., Schnell, E., and Barkai, E. (1995). Dynamics of learning and recall at excitatory recurrent synapses and cholinergic modulation in rat hippocampal region Ca3. *J. Neurosci.* 15: 5249–5262.

Hjorth-Simonsen, A. (1973). Some intrinsic connections of the hippocampus in the rat: An experimental analysis. *J. Comp. Neurol.* 147: 145–161.

Huerta, P.T. and Lisman, J.E. (1993). Heightened synaptic plasticity of hippocampal CA1 neurons during a cholinergically induced rhythmic state. *Nature* 364: 723–725.

Huerta, P.T. and Lisman, J.E. (1995). Bidirectional synaptic plasticity induced by a single burst during cholinergic theta oscillation in CA1 in vitro. *Neuron* 15: 1053–1063.

Hyman, J.M., Wyble, B.P., Goyal, V., Rossi, C.A., and Hasselmo, M.E. (2003). Stimulation in hippocampal region CA1 in behaving rats yields long-term potentiation when delivered to the peak of theta and long-term depression when delivered to the trough. *J. Neurosci.* 23: 11725–11731.

Iijima, T., Witter, M.P., Ichikawa, M., Tominaga, T., Kajiwara, R., and Matsumoto, G. (1996). Entorhinal-hippocampal interactions revealed by real-time imaging. *Science* 272: 1176–1179.

Ishizuka, N., Weber, J., and Amaral, D.G. (1990). Organization of intrahippocampal projections originating from CA3 pyramidal cells in the rat. *J. Comp. Neurol.* 295: 580–623.

Jensen, O. and Tesche, C.D. (2002). Frontal theta activity in humans increases with memory load in a working memory task. *Eur. J. Neurosci.* 15: 1395–1399.

Kahle, J.S. and Cotman, C.W. (1989). Carbachol depresses synaptic responses in the medial but not the lateral perforant path. *Brain Res.* 482: 159–163.

Konopacki, J., Maciver, M.B., Bland, B.H., and Roth, S.H. (1987). Theta in hippocampal slices: Relation to synaptic responses of dentate neurons. *Brain Res. Bull.* 18: 25–27.

Kopell, N., Ermentrout, G.B., Whittington, M.A., and Traub, R.D. (2000). Gamma rhythms and beta rhythms have different synchronization properties. *Proc. Natl. Acad. Sci. U. S. A.* 97: 1867–1872.

Landfield, P.W., McGaugh, J.L., and Tusa, R.J. (1972). Theta rhythm: A temporal correlate of memory storage processes in the rat. *Science* 175: 87–89.

Larson, J. and Lynch, G. (1986). Induction of synaptic potentiation in hippocampus by patterned stimulation involves two events. *Science* 232: 985–988.

Larson, J., Wong, D., and Lynch, G. (1986). Patterned stimulation at the theta frequency is optimal for the induction of hippocampal long-term potentiation. *Brain Res.* 368: 347–350.

Leung, L.W., Lopes da Silva, F.H., and Wadman, W.J. (1982). Spectral characteristics of the hippocampal EEG in the freely moving rat. *Electroencephalog. Clin. Neurophysiol.* 54: 203–219.

Leung, L.S. (1992). Fast (beta) rhythms in the hippocampus: A review. *Hippocampus* 2: 93–98.

Leung, L.S. (1998). Generation of theta and gamma rhythms in the hippocampus. *Neurosci. Biobehav. Rev.* 22: 275–290.

Levey, A.I., Edmunds, S.M., Koliatsos, V., Wiley, R.G., and Heilman, C.J. (1995). Expression of m1–m4 muscarinic acetylcholine receptor proteins in rat hippocampus and regulation by cholinergic innervation. *J. Neurosci.* 15: 4077–4092.

Lisman, J., Jensen, O., and Kahana, M. (2001). Toward a physiologic explanation of behavioral data on human memory—The role of theta-gamma oscillations and NMDAR-dependent LTP. In: Holscher, C., ed., *Neuronal Mechanisms of Memory Formation: Concepts of Long-Term Potentiation and Beyond*, Cambridge University Press, Cambridge, pp.195–223.

Madison, D.V., Lancaster, B., and Nicoll, R.A. (1987). Voltage clamp analysis of cholinergic action in the hippocampus. *J. Neurosci.* 7: 733–741.

M'Harzi, M. and Jarrard, L.E. (1992). Effects of medial and lateral septal lesions on acquisition of a place and cue radial maze task. *Behav. Brain Res.* 49: 159–165.

Mizumori, S.J., Perez, G.M., Alvarado, M.C., Barnes, C.A., and McNaughton, B.L. (1990). Reversible inactivation of the medial septum differentially affects two forms of learning in rats. *Brain Res.* 528: 12–20.

Nakajima, Y., Nakajima, S., Leonard, R.J., and Yamaguchi, K. (1986). Acetylcholine raises excitability by inhibiting the fast transient potassium current in cultured hippocampal neurons. *Proc. Natl. Acad. Sci. U. S. A.* 83: 3022–3026.

Nicholson, C. (1973). Theoretical analysis of field potentials in anisotropic ensembles of neuronal elements. *IEEE Trans. Biomed. Eng.* 20: 278–288.

Nicholson, C. and Freeman, J.A. (1975). Theory of current source-density analysis and determination of conductivity tensor for anuran cerebellum. *J. Neurophysiol.* 38: 356–368.

Nicholson, C. and Llinas R. (1975). Real time current source-density analysis using multi-electrode array in cat cerebellum. *Brain Res.* 100: 418–424.

Pavlides, C., Greenstein, Y.J., Grudman, M., and Winson, J. (1988). Long-term potentiation in the dentate gyrus is induced preferentially on the positive phase of theta-rhythm. *Brain Res.* 439: 383–387.

Pitler, T.A. and Alger, B.E. (1992). Cholinergic excitation of GABAergic interneurons in the rat hippocampal slice. *J. Physiol.* 450: 127–142.

Qian, J. and Saggau P. (1997). Presynaptic inhibition of synaptic transmission in the rat hippocampus by activation of muscarinic receptors—Involvement of presynaptic calcium influx. *Brit. J. Pharmacol.* 122: 511–519.

Sheridan, R.D. and Sutor, B. (1990). Presynaptic M1 muscarinic cholinoceptors mediate inhibition of excitatory synaptic transmission in the hippocampus in vitro. *Neurosci. Lett.* 108: 273–278.

Shimono, K., Brucher, F., Granger, R., Lynch, G., and Taketani, M. (2000). Origins and distribution of cholinergically induced beta rhythms in hippocampal slices. *J. Neurosci.* 20: 8462–8473.

Shimono, K., Kubota, D., Brucher, F., Taketani, M., and Lynch, G. (2002). Asymmetrical distribution of the Schaffer projections within the apical dendrites of hippocampal field CA1. *Brain Res.* 950: 279–287.

Staubli, U. and Lynch, G. (1987). Stable hippocampal long-term potentiation elicited by 'theta' pattern stimulation. *Brain Res.* 435: 227–234.

Swanson, L.W., Wyss, J.M., and Cowan, W.M. (1978). An autoradiographic study of the organization of intrahippocampal association pathways in the rat. *J. Comp. Neurol.* 181: 681–715.

Tesche, C.D. and Karhu, J. (2000). Theta oscillations index human hippocampal activation during a working memory task. *Proc. Natl. Acad. Sci. U. S. A.* 97: 919–924.

Traub, R.D., Whittington, M.A., Buhl, E.H., Jefferys, J.G.R., and Faulkner, H.J. (1999). On the mechanism of the gamma -> beta frequency shift in neuronal oscillations induced in rat hippocampal slices by tetanic stimulation. *J. Neurosci.* 19: 1088–1105.

Valentino, R.J. and Dingledine, R. (1981). Presynaptic inhibitory effect of acetylcholine in the hippocampus. *J. Neurosci.* 1: 784–792.

van der Linden, S., Panzica, F., and de Curtis, M. (1999). Carbachol induces fast oscillations in the medial but not in the lateral entorhinal cortex of the isolated guinea pig brain. *J. Neurophysiol.* 82: 2441–2450.

Vertes, R.P. and Kocsis, B. (1997). Brainstem-diencephalo-septohippocampal systems controlling the theta rhythm of the hippocampus. *Neuroscience* 81: 893–926.

Whittington, M.A., Traub, R.D., and Jefferys, J.G.R. (1995). Synchronized oscillations in interneuron networks driven by metabotropic glutamate receptor activation. *Nature* 373: 612–615.

Williams, J.H. and Kauer, J.A. (1997). Properties of carbachol-induced oscillatory activity in rat hippocampus. *J. Neurophysiol.* 78: 2631–2640.

Winson, J. (1978). Loss of hippocampal theta rhythm results in spatial memory deficit in the rat. *Science* 201: 160–163.

Yamamoto, C. and Kawai, N. (1967). Presynaptic action of acetylcholine in thin sections from the guinea pig dentate gyrus in vitro. *Exp. Neurol.* 19: 176–187.